THE JOURNAL OF PHYSICAL CHEMISTRY C

pubs.acs.org/JPCC Article

High-Pressure Synthesis of Cyclic Phosphazenes by Near-UV Photoinduced Reactivity of NH_3 and Elemental Phosphorus

Demetrio Scelta,* Adhara Baldassarre, Manuel Serrano-Ruiz, Alexey Marchuk, Sebastian Vogel, Wolfgang Schnick, Maurizio Peruzzini, Roberto Bini, and Matteo Ceppatelli

Cite This: https://dx.doi.org/10.1021/acs.jpcc.9b11462 Read Online

ACCESS | Metrics & More | Article Recommendations

ABSTRACT: A comparison between the high-pressure (0.8 GPa) photoinduced reactivity of black and red phosphorus at ambient temperature in the presence of ammonia has been conducted in diamond anvil cells (DACs), using spectroscopy (IR and Raman) and X-ray diffraction (XRD). Reactivity has been triggered exploiting the two-photon absorption of near-UV radiation by ammonia. The infrared characterization showed a very complex reactivity in the case of red phosphorus, proceeding to a much higher extent with respect to the black allotrope. Furthermore, Raman spectra showed the formation of molecular hydrogen and phosphine besides three different solid products. Whereas one of them is air sensitive, the other two are recoverable at ambient conditions. IR, Raman, and XRD data for the obtained products have been compared to those acquired on known $H_xP_yN_z$ compounds: for one of the two stable products, a fair matching was found with the XRD pattern and the IR spectrum of $P_3N_3(NH_2)_6\cdot(NH_3)_{0.5}$, whereas for the other one only the functional groups actually involved in the structure could be evinced from accurate Raman mapping of the sample, with no further information about composition or stoichiometry. High density conditions in combination with near-UV laser irradiation were thus proved to be effective in the formation of two stable reaction products featuring new P−N functionalities, both recoverable at ambient pressure. For the first time, a cyclic triphosphazene has been synthesized through the reaction of red phosphorus and ammonia triggered by UV light under moderate high-pressure conditions, possibly opening new perspectives about this topic.

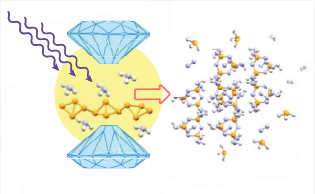

■ INTRODUCTION

Three main allotropes of phosphorus exist at ambient pressure, roughly identified by their colors:[1] white phosphorus (P_{white}), black phosphorus (P_{black}), and red phosphorus (P_{red}), of which several forms with different morphology, ranging from amorphous to crystalline (gray, violet, or brown), are known (*I*−*V*).[2]

P_{white}, made of tetrahedral-shaped molecular P_4 units, is the most widely used allotrope of phosphorus, despite its instability, high reactivity, flammability, and toxicity. On the other hand, P_{red} is a polymeric amorphous solid, much more stable and less toxic than P_4: despite the fact that using P_{red} would be preferable over P_4 in both industrial and research chemistry, this allotrope has found few technological applications over the years mainly in the matches industry or as a flame retardant additive for a large variety of plastic materials.[3] At ambient temperature and pressures above 6.6 GPa[4−6] or at temperature above 1000 K and pressures of about 1 GPa,[7] an interconversion of P_{red} to P_{black} is reported to occur. The phase diagram of phosphorus is well-known at ambient *T* up to pressures of 340 GPa.[4,8−11] P_{black} is thermodynamically the most stable allotrope of the element.[1] It was first synthesized by Bridgman at 1.20 GPa and 473 K in 1914.[12] P_{black} is a layered, crystalline solid with orthorhombic structure (A17, space group *Cmca*, *Z* = 8) and stable at room temperature from ambient pressure to about 4.5 GPa.[13] P_{black} is actually attracting great interest in the scientific community due to the extraordinary properties of its monolayer, called phosphorene (in analogy with the graphite−graphene system).[14] Upon compression above 4.5 GPa, P_{black} transforms into a second layered structure (rhombohedral A7, space group $R\bar{3}m$, *Z* = 2).[15,16] A7 is stable up to about 10.5 GPa, where recently a layered pseudosimple cubic structure (p-sc) has been demonstrated to exist instead of the previously reported, nonlayered simple cubic one (sc, space group $Pn\bar{3}m$, Z = 1), thus extending the pressure range where layered phases of P_{black} can be stabilized up to about 30 GPa.[13,17] Above this threshold, the sc phase forms and extends up to about 107 GPa.[18]

As the high-pressure reactivity is concerned, the photo-activated chemistry of P_{red} has been studied in the presence of H_2O[19] and EtOH[20] with interesting results, particularly regarding the formation of molecular hydrogen. Being well-known that high density conditions, together with electronic

Received: December 11, 2019
Revised: January 9, 2020
Published: January 13, 2020

photoexcitation, are able to trigger a chemical reactivity in diverse molecular systems, an interesting task is represented by the investigation of the structural effects, in terms of amorphous versus layered structure, on the high-pressure chemistry of phosphorus. Within this framework, it is natural to focus on the high-pressure photoinduced reactivity of polymeric amorphous P_{red} and layered crystalline P_{black} in the presence of a simple reactive N-bearing molecule-like ammonia (NH_3), with the purpose of fostering the N-functionalization of phosphorus and the synthesis of new P- and N-containing compounds.

NH_3 has a very well-known high-pressure behavior and phase diagram,[21,22] and its electronic structure is quite similar to that of H_2O. Photoinduced reactivity can be triggered by exploiting the quasi-dissociative character of the first excited electronic state of NH_3,[23−26] which shows a very weak dissociation barrier that can be overcome by the two-photon (TP) absorption of near-UV radiation ($\lambda \simeq 350$ nm), resulting in the formation of a H atom and NH_2 excited fragment, following[27]

$$NH_3 + h\nu \rightarrow H + NH_2(\tilde{X}(^2B_1))$$

In more detail, from the ground electronic state $\tilde{X}(^1A_1')$, the system can reach the first excited state $\tilde{A}(^1A_2'')$ (the required energy, 216.7 nm, is largely exceeded via the TP absorption of 350 nm wavelength). $\tilde{A}(^1A_2'')$ is a predissociative state with a weakly bonded planar trigonal structure that, depending on the vibrational excitation, could evolve in a bond cleavage with the production of $H(^2S)$ and NH_2 fragments, the latter in both its excited $\tilde{A}(^2A_1)$ or ground state $\tilde{X}(^2B_1)$.[23,25,26]

Previous literature studies have shown how this low-lying electronic excited state can be exploited to induce the chemical functionalization of a solid substrate, with the formation of new N-bearing functionalities.[28,29] The idea behind this study is to generate highly reactive fragments under high density conditions provided by pressure, where the reduced molecular distances make the time scale for the recombination process of the photoactivated species and for the effective intermolecular collisions comparable, possibly resulting in a nitrogen functionalization of phosphorus. Within this picture, a comparison between the high-pressure photoinduced reactivity of P_{red}/NH_3 and P_{black}/NH_3 mixtures is mandatory to explore the reactive properties of the different structures of phosphorus and to probe the stability of the layered crystal structure with respect to the amorphous nonlayered one. Moreover, the scientific community is currently looking with great attention at hydrides of light elements for their properties as high-pressure superconductors[30−33] and high hydrogen content materials for energy storage purposes.[34] The synthesis and subsequent characterization of the high-pressure behavior of novel hydrides obtained from elemental phosphorus using ammonia as the source of both N and H could have profound implications in these extremely active research fields.

■ EXPERIMENTAL SECTION

A membrane diamond anvil cell (mDAC) equipped with IIa-type diamonds was employed to pressurize the samples. The samples were enclosed by a stainless steel gasket with initial diameter and thickness of about 150 and 50 μm, respectively. Amorphous P_{red} powder (from Aldrich, 99.99+% purity) was first loaded in the gasket hole, which was then filled with NH_3. The black phosphorus sample was prepared by pressurizing P_{red} at ambient temperature above 6.6 GPa.[4−6] Gaseous NH_3 was condensed directly between the diamonds, into the gasket hole, by means of the *spray-loading* technique.[35] The pressure was measured by the ruby fluorescence method.[36,37] Reactivity was triggered by focusing the UV multiline emission (≈350 nm) of an Ar ion laser onto the sample with a power of 500 mW in successive irradiations of variable durations (from 1 h to a maximum of 15 h per irradiation). Raman spectra were measured in back scattering geometry by focusing a few mW of the 647.1 nm line of a Kr ion laser onto the sample through a long working distance 20× Mitutoyo micro-objective providing a beam spot diameter of 2−3 μm. The high spatial resolution of the Raman equipment, together with the complete automation of the DAC stage (remotely controlled), was allowed to perform grid acquisitions on the sample (Raman mappings): in this procedure, a certain number of Raman acquisitions can be performed at definite positions on a square mesh of desired dimensions. The unpolarized scattered light was dispersed by a single-stage monochromator (Acton/SpectraPro 2500i), equipped with holographic super notch filters, and detected by a CCD detector (Princeton Instruments Spec-10:100BR). The typical resulting instrumental resolution was 0.6 cm^{-1} with the employed wavelength. More details on the Raman setup can be found elsewhere.[38] Raman data were analyzed using Fityk software.[39] FTIR absorption measurements were performed using a Bruker-IFS 120 HR spectrometer suitably modified for high-pressure and high=-temperature experiments,[40] with an instrumental resolution of 1 cm^{-1}. The powder X-ray diffraction patterns (PXRD) were acquired at an ESRF ID27 high-pressure dedicated beamline,[41] using a monochromatic radiation (wavelength λ = 0.3738 Å) with beam spot size diameter of 5 μm, that allows a sufficiently accurate spatial mapping of the sample, and a MAR CCD165 detector. The typical acquisition time was 20 s with a total oscillation of 10 degrees. The detector tilt and sample to detector distance were determined by a CeO_2 standard. The raw images were processed using DIOPTAS software,[42] and the PXRD patterns were analyzed using GSAS-II software.[43]

■ RESULTS AND DISCUSSION

After loading, the samples were compressed to 0.8 GPa and irradiated. At this pressure NH_3 is fluid, thus assuring a higher mobility for the photogenerated species and at the same time providing sufficient high density conditions. As mentioned in the Experimental Section, to study the P_{black}/NH_3 mixture a sample loaded with pristine P_{red} was compressed above 6.6 GPa to induce the conversion of P_{red} to P_{black}. The successful formation of P_{black} was confirmed by the Raman spectra.[4−6] The samples were then decompressed to 0.8 GPa before the irradiation. No traces of reactivity with NH_3 were observed under pure compression in the FTIR and Raman spectra.

Reactivity was photoinduced in both mixtures, although to a very different extent. On the P_{black}/NH_3 mixture, seven irradiations were performed at 0.8 GPa and ambient temperature with 500 mW of UV light ($\lambda \simeq 350$ nm) for a total of 67 h. On the P_{red}/NH_3 mixture, five irradiations of the same laser power in the same p,T conditions were performed, for a total of 59 h. Figures 1 and 2 report the FTIR spectra acquired during the experiments on P_{black}/NH_3 and P_{red}/NH_3 mixtures, respectively. On top of the spectra, microscope photographs of the P_{black}/NH_3 and P_{red}/NH_3 samples at successive stages of transformation are shown. For the P_{red}/NH_3 mixture, the product of the photoinduced reaction has

https://dx.doi.org/10.1021/acs.jpcc.9b11462
J. Phys. Chem. C XXXX, XXX, XXX−XXX

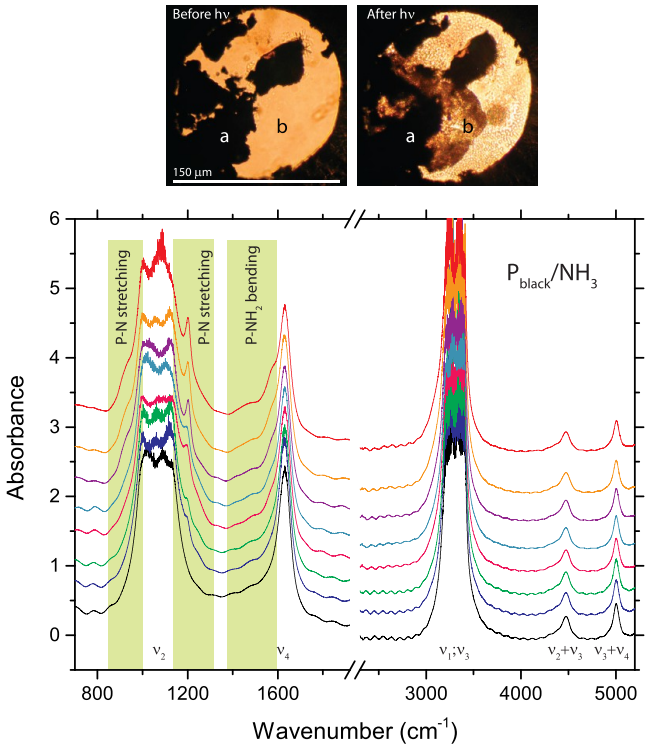

Figure 1. Top: microscope photographs of the P_{black}/NH_3 sample at 0.8 GPa before (left) and after (right) the photoinduced reaction. (a) and (b) labels refer to the points where starting and reacted sample were characterized by Raman spectroscopy (see text). Bottom: sequence of the FTIR spectra acquired during the photoinduced reaction between P_{black} and NH_3, from bottom to top: before irradiation (black); after first irradiation, 1 h (blue); after second irradiation, 2 h (green); after third irradiation, 7 h (pink); after fourth irradiation, 14 h (light cyan); after fifth irradiation, 14 h (violet); after sixth irradiation, 14 h (orange); and after seventh irradiation, 15 h (red). All the irradiations were performed at 0.8 GPa using 500 mW of the 350 nm line, for a total of 67 h. Yellow-green shaded areas highlight the frequency regions where new absorption bands appeared. The normal vibrational modes of NH_3 and their combination modes are also marked. The spectra were vertically shifted for the sake of clarity, and therefore their absorbance units have to be intended as relative. The wavenumber axis break excludes the region where the saturating absorption of the diamond anvils occurs.

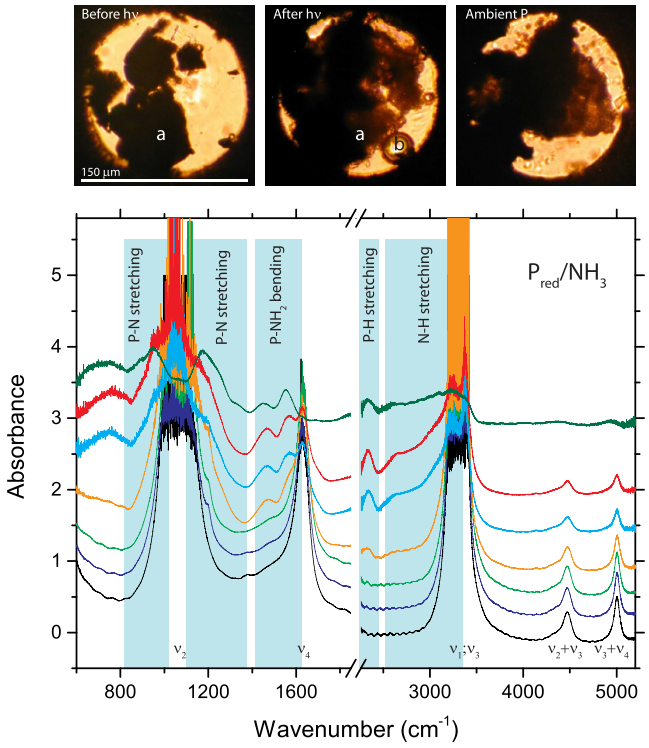

Figure 2. Top: microscope photographs of the P_{red}/NH_3 sample at 0.8 GPa before (left) and after (middle) the irradiations and after releasing pressure (right). (a) and (b) labels refer to the points where pristine and reacted sample were characterized by Raman spectroscopy (see text). Bottom: sequence of the FTIR spectra acquired during the photoinduced reaction between P_{red} and NH_3, from bottom to top: before irradiation (black); after first irradiation, 5 h (blue); after second irradiation, 14 h (green); after third irradiation, 14 h (orange); after fourth irradiation, 15 h (cyan); after fifth irradiation, 11 h (red); and recovered sample after releasing pressure (dark green). All the irradiations were performed at 0.8 GPa using 500 mW of the 350 nm line, for a total of 59 h. Cyan shaded areas highlight the frequency regions where new absorption bands appeared. The normal vibrational modes of NH_3 and their combination modes are also marked. Spectra were vertically shifted for the sake of clarity, and therefore their absorbance units have to be intended as relative. The wavenumber axis break excludes the region where the saturating absorption of the diamond anvils occurs.

been recovered at ambient conditions and an FTIR spectrum acquired (green trace in Figure 2).

The dark areas of the samples in the optical images of Figures 1 and 2, acquired before irradiation, correspond to the starting P_{black} or P_{red} and the surrounding, transparent areas to bulk NH_3. The dark and transparent areas were previously characterized by Raman spectroscopy, and the spectra were found to be in perfect agreement with those reported in the literature for NH_3,[44−47] P_{red},[4] and P_{black}.[48] Upon successive irradiations, the visual aspect of the samples progressively changed. After the last one, small bubbles and an extended grainy region appeared in the P_{black}/NH_3 sample, thus suggesting the occurrence of some reactivity in the regions where P_{black} was in contact with NH_3 (see Figure 1). On the other hand, far more dramatic changes could be observed in the P_{red}/NH_3 sample: big bubbles appeared in the bulk; the transparent NH_3 region and a large portion of the starting P_{red} became noticeably consumed; and the grainy, eroded portions of the sample, where solid products were found, were retained after releasing pressure (right image in Figure 2) and then further spectroscopically and structurally characterized.

Infrared Spectroscopy. FTIR spectroscopy was used to monitor the evolution of the reactions and the formation of products. The initial FTIR spectra for both mixtures (Figure 1 and 2) were dominated by the saturated bands related to the fundamental modes of NH_3:[45−47] $\nu_2(A_1)$ at about 1058 cm^{-1}, $\nu_4(E)$ at 1630 cm^{-1}, and the overlapping $\nu_1(A_1)$ and $\nu_3(E)$ modes at ∼3307 cm^{-1}. At higher frequency, the combination modes $\nu_2 + \nu_3$ at 4470 cm^{-1} and $\nu_3 + \nu_4$ at 5003 cm^{-1} were found. No IR bands related to P_{black} or P_{red} were visible in the mid infrared spectrum. For both P_{black}/NH_3 and P_{red}/NH_3 mixtures, upon irradiations we observed the appearance of new absorption bands, highlighted by the shaded areas in Figures 1 and 2. In P_{black}/NH_3, immediately after the first irradiation (500 mW, 1 h, blue trace in Figure 1), the appearance of a shoulder on the high-frequency side of ν_2 absorption of NH_3 can be appreciated. This band, centered at about 1200 cm^{-1},

https://dx.doi.org/10.1021/acs.jpcc.9b11462
J. Phys. Chem. C XXXX, XXX, XXX−XXX

which intensified upon further irradiations, could be assigned to stretching vibrations suggesting the formation of new chemical bonds involving P and N,[49] like other spectroscopic signatures appeared during the irradiations as a broad absorption in the 850−1000 cm^{-1} region on the low-frequency side of the ν_2 band of ammonia. The two broad bands at 1500 and 1550 cm^{-1} were assigned to the bending modes of newly formed N−H in P−NH_2 groups.

In the P_{red}/NH_3 sample, a more complex and higher reactivity was observed with respect to that found in P_{black}/NH_3 (Figure 2): the spectra showed the appearance of a shoulder on the high-frequency side of the $\nu_2(A_1)$ band of NH_3 at about 1200 cm^{-1}, a broad band between 700 and 950 cm^{-1}, two bands centered at 1500 and 1550 cm^{-1}, and another broad one centered at 2345 cm^{-1}. The bands at 700−950, 1200, 1500, and 1550 cm^{-1} can be assigned to P−N stretching modes and P−NH_2 bending mode, whereas the absorption band appearing at 2345 cm^{-1} can be assigned to stretching modes of P−H groups.

The comparison of the FTIR spectra before and after the irradiations (black and red traces in Figures 1 and 2) allows us to estimate the consumption of NH_3 by the ratio of the integrated absorption of the $\nu_2 + \nu_3$ and $\nu_3 + \nu_4$ combination modes and, consequently, the extent of the reaction. The consumption of NH_3 with respect to its starting amount was 21% in the case of P_{black}/NH_3 and 72% in the case of P_{red}/NH_3, indicating a remarkably higher reactivity of the P_{red}/NH_3 mixture with respect to the P_{black}/NH_3 one. This is likely related to the different structural properties of crystalline P_{black} and amorphous P_{red}. Particularly, the larger surface area in P_{red}[50] offers a higher density of reactive sites compared to P_{black},[51] where in addition NH_3 cannot penetrate between the layers.[17]

The product of the P_{red}/NH_3 reaction was recovered at ambient pressure and an FTIR spectrum acquired under vacuum, before any exposure to air (Figure 2, dark green trace). On opening the cell, the saturating absorption bands of unreacted NH_3 disappeared, and the remaining absorption bands of the solid product could be clearly identified: two asymmetric broad peaks at 985 and 1200 cm^{-1}, a doublet at 1453 and 1556 cm^{-1}, the P−H stretching peak at 2345 cm^{-1}, and a broad absorption in the region from 2600 to 3500 cm^{-1} related to N−H stretching modes.

Raman Spectroscopy and Raman Mapping. Raman spectroscopy provides useful indications about the nature of the reaction products. In the case of P_{black}/NH_3, the lower reactivity is reflected in minor modifications of the Raman spectra. Figure 3 reports the Raman spectra acquired before and after irradiations in the a and b points of the sample (see microscope photographs therein) in two different spectral ranges. In the left panel, the Raman-active modes of P_{black} are visible (point a, black trace): B_{1g} at 191.6 cm^{-1} and B_{3g} at 226.6 cm^{-1} modes, the two A_g modes (363.4 and 459.3 cm^{-1}), and finally the B_{2g} mode (431.6 cm^{-1}).[48,52] Upon irradiation (point a, red trace), minor changes were observed between 190 and 400 cm^{-1}. On bulk NH_3 (point b), besides the diffuse scattering typical of fluid ammonia, a broad doublet with peak frequencies at 675 and 710 cm^{-1} appeared upon irradiation, together with two broader and weaker bands at 575 and 824 cm^{-1}. This is the spectral range where the bands due to P−H bending modes are expected. In the right panel of Figure 3, showing the spectral range between 2000 and 2700 cm^{-1}, the characteristic sharp Raman band related to P−H stretching of

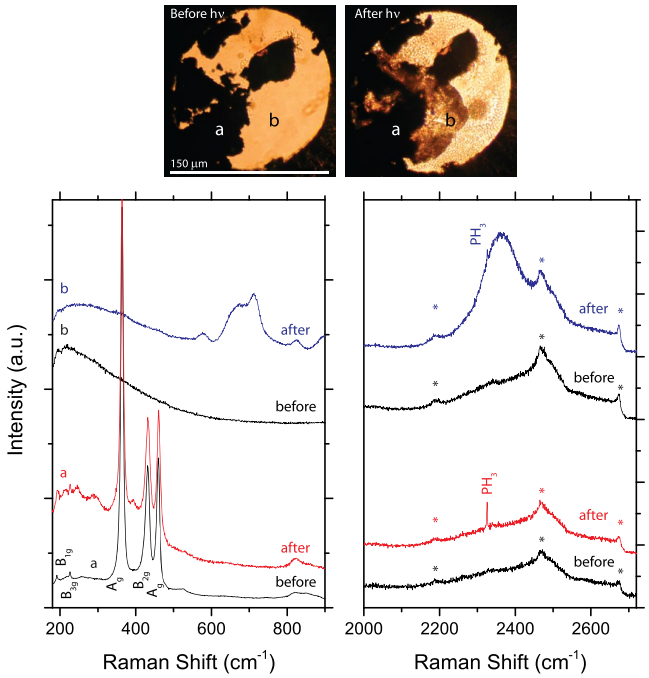

Figure 3. Raman spectra of the P_{black}/NH_3 sample before and after the irradiations. Top: microscope photographs of the P_{black}/NH_3 sample at 0.8 GPa before (left) and after (right) the photoinduced reaction. Bottom left: Raman spectra in the low-frequency range acquired on P_{black} (a) and on bulk NH_3 (b) before (black traces) and after (red and blue traces) irradiations. Bottom right: Raman spectra in the 2000−2700 cm^{-1} frequency range, acquired on P_{black} (a) and on bulk NH_3 (b), before (black traces) and after (red and blue traces) irradiations. Asterisks refer to Raman peaks from the diamond anvils. Spectra were vertically shifted for the sake of clarity.

phosphine (PH_3) was found at 2325.1 cm^{-1} on both points a and b of the sample. In this region of the sample, however, the phosphine P−H stretching band is superimposed to a much broader and intense Raman band, centered at about 2366 cm^{-1}, likely due to the stretching mode of new different P−H groups. No other significant features can be appreciated in Raman spectra of the P_{black}/NH_3 mixtures.

In the P_{red}/NH_3 sample, instead, a much more complex chemical reactivity occurred. The high spatial resolution of the Raman setup allowed us to investigate three different regions of the sample: a solid region (starting P_{red} and grainy product), a transparent fluid region (bulk NH_3), and several bubbles. Figures 4 and 5 show the Raman spectra collected in these different regions of the sample.

Figure 4 reports the Raman spectra acquired in three different spectral ranges on bubbles (point b in the central microscope photo). The four intense rotational bands of molecular hydrogen ($S_0(0)$ at 357.5 cm^{-1}, $S_0(1)$ at 590 cm^{-1}, $S_0(2)$ at 818.1 cm^{-1}, and $S_0(3)$ at 1038.6 cm^{-1})[53,54] and the H−H stretching band at 4167 cm^{-1} attested for the production of H_2 during the photoinduced reaction of P_{red} and NH_3. As in the case of P_{black}, but to a larger extent, Raman spectra also confirmed the formation of PH_3, indicated by the intense band centered at 2328 cm^{-1}. Both H_2 and PH_3 were known to form in analogous experiments on P_{red}/H_2O mixtures and, to a less extent, P_{red}/EtOH mixtures.[19,20]

More intriguing and complementary information can be gained looking at the dark areas of the sample where P_{red} transformed into other solid products upon irradiation. To

https://dx.doi.org/10.1021/acs.jpcc.9b11462
J. Phys. Chem. C XXXX, XXX, XXX−XXX

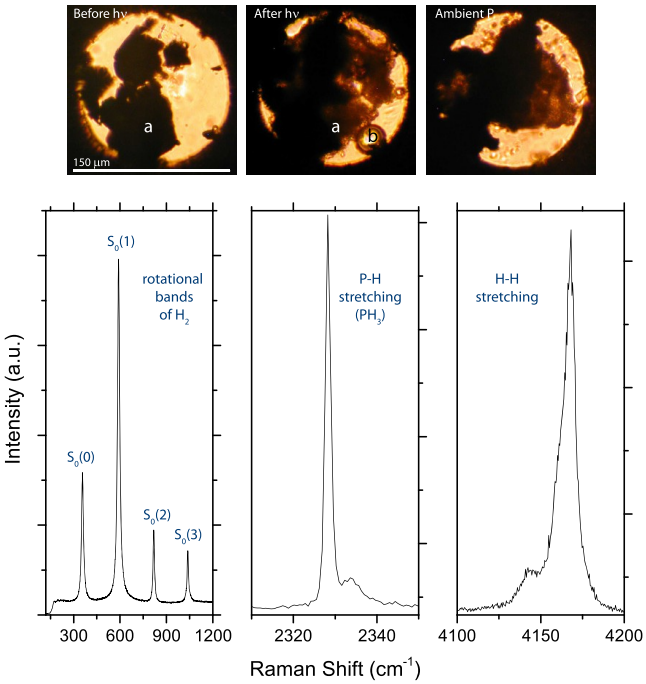

Figure 4. Top: microscope photographs of the P_{red}/NH_3 sample at 0.8 GPa before (left) and after (center) irradiations and after releasing pressure (right). Bottom: selected frequency regions of the Raman spectra acquired on the bubbles visible in the central photo (point b) after P_{red}/NH_3 irradiation at 0.8 GPa, showing the rotational bands of molecular H_2 (left) and the vibrational stretching bands of phosphine PH_3 (center) and molecular H_2 (right).

perform a deeper spectroscopic and structural characterization of the products, a second sample was prepared (see microscope photographs in Figure 5), and the reactivity was induced under the same p,T and laser irradiation conditions. Three very different Raman profiles, possibly related to three different solid products, hereafter indicated as Product 1, Product 2, and Product 3 (see colored points on the grids overimposed to the optical photographs of the sample in Figures 5 and 6), emerged from accurate Raman mapping of the sample area, performed at 0.6 GPa and at ambient conditions in three different spectral ranges (Figure 6). The right panel in Figure 5 shows the Raman spectra of the three different products together with the Raman spectra of P_{red}[4] and P_{black}[48] (acquired at the beginning of the experiments) in the 200−1200 cm^{-1} spectral window.

The red trace refers to the spectrum of Product 1 at 0.6 GPa, featuring a band at 224 cm^{-1}, a doublet at 281 and 297 cm^{-1}, the most intense peak at 337 cm^{-1}, other less intense peaks at 380 and 409 cm^{-1}, and finally, a doublet at 453 and 471 cm^{-1}. Product 2 (blue trace in Figure 5) has a completely different spectrum, resembling that of a molecular crystal: a broad, weak, and structured profile between 200 and 400 cm^{-1}, likely due to lattice modes, and two strong and sharp bands at 545 and 725 cm^{-1}, ascribable to internal modes. Both products 1 and 2 were recovered at ambient conditions. Finally, Product 3 (green traces) shows a broad doublet at 670−725 cm^{-1} at 0.6 GPa, but on releasing pressure and opening the cell its spectrum dramatically changes, indicating its transformation to H_3PO_3 (upper trace in Figure 5).[19] In any case, no matching was found between the Raman spectra of the three products and those of P_{red} or P_{black}.

The complete Raman mapping, performed in three different spectral ranges to cover the whole spectrum between 200 and 3500 cm^{-1}, is reported in Figure 6 and allows us to correlate the various products with the presence of different functional groups, shedding light on their composition. The comparison of the maps indicates that Product 3 is distributed at the edges

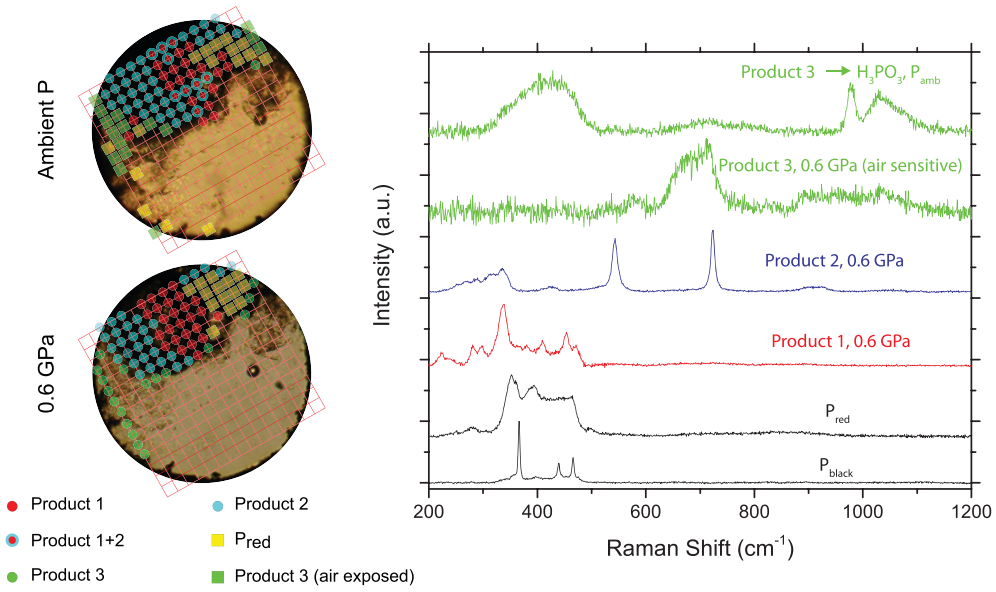

Figure 5. Left: microphotographs of the sample acquired after irradiation of the P_{red}/NH_3 mixture at 0.6 GPa (bottom) and of the recovered sample at ambient conditions (top). The superimposed red grids correspond to the acquisition points of the Raman mappings, consisting of a 16 × 16 matrix with 5 μm spatial resolution (for each point of the grid three spectral regions were sampled, see Figure 6). Right: selected significant Raman spectra of the solid products (red, blue, and green traces) acquired during the mapping in the 200−1200 cm^{-1} frequency range at 0.6 GPa, compared with Raman spectra of P_{black} and P_{red} at ambient conditions (black traces). The upper trace refers to the Raman spectrum of Product 3 after releasing pressure. The colors of the Raman spectra correspond to the colors of the points in the maps, as indicated by the legend below the microscope images: Product 1 is highlighted in red, Product 2 in blue, and Product 3 in green. Unreacted P_{red} is indicated by yellow squares.

https://dx.doi.org/10.1021/acs.jpcc.9b11462
J. Phys. Chem. C XXXX, XXX, XXX−XXX

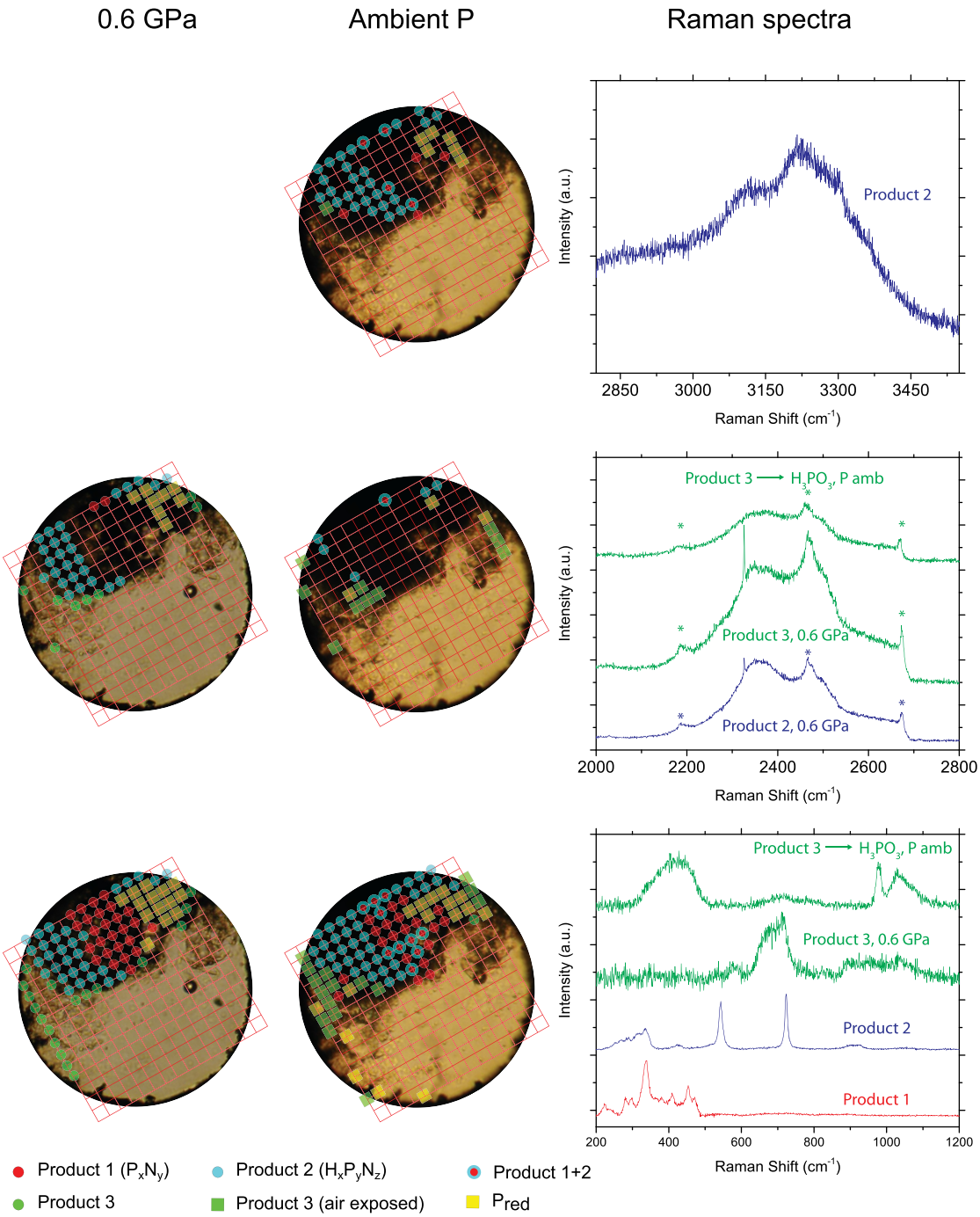

Figure 6. Microphotographs of the sample acquired after irradiation of the P_{red}/NH_3 mixture at 0.6 GPa (left column) and of the recovered sample at ambient pressure (center column), with the superimposition of red grids corresponding to the acquisition points of the Raman mapping in three spectral regions, together with a selection of Raman spectra (right column) for each spectral region (200−1200 cm^{-1} bottom, 2000−2800 cm^{-1} middle, 2800−3500 cm^{-1} top). The colors of the Raman spectra correspond to the colors of the points in the maps, as indicated by the legend below the microscope images: Product 1 is highlighted in red, Product 2 in blue, and Product 3 in green. Unreacted P_{red} is indicated by yellow squares. The spectra, normalized to the most intense band, are vertically translated for the sake of clarity. Asterisks in the spectra of the middle right panel refer to Raman peaks from the diamond anvils.

of the solid region, where a grainy solid is visible: the edges of the solid portion of the sample were the first part to deteriorate in contact with the atmospheric moisture, and Product 3 rapidly turned into H_3PO_3 (from green circles to green squares in the maps).[19] The solid portion of the sample seems equally divided in three parts, one with a major presence of Product 1 (red), one prevalently containing Product 2 (blue), and the other one mostly made of unreacted P_{red} (yellow). Besides the 200−1200 cm^{-1} region, the higher-frequency spectral ranges give very interesting hints about the actual compositions of Product 1 and Product 2 (Figure 6).

At 0.6 GPa, the Raman spectra acquired between 2000 and 2800 cm^{-1} revealed the presence of phosphine everywhere in the sample (not reported on the maps). In some points, corresponding to the regions of the sample where products 2 and 3 were found (Figure 6, middle right panel, blue and green

https://dx.doi.org/10.1021/acs.jpcc.9b11462
J. Phys. Chem. C XXXX, XXX, XXX−XXX

traces), the narrow P−H stretching band of phosphine was present together with a broader band centered at about 2360 cm^{-1}, assigned to the stretching of other P−H bonds. Once the DAC was opened, the broad P−H stretching band disappeared everywhere in the sample except where H_3PO_3 can be found, suggesting it to be likely related to the air-sensitive Product 3. Interestingly, a clear correspondence in the spatial distribution of the N−H band in the spectral range between 2800 and 3500 cm^{-1} with the spatial distribution of Product 2 (blue points and traces in Figure 6) emerging from the Raman mappings in the 200−1200 cm^{-1} and 2000−2800 cm^{-1} spectral ranges is observed, indicating that Product 2 features N−H functionalities. To summarize, Product 3 was identified as an amorphous, air-sensitive product characterized by the presence of P−H functionalities, which could not be recovered at ambient conditions due to its decomposition to H_3PO_3 in contact with atmospheric moisture.[19] Products 1 and 2 exhibit Raman bands in the 200−1200 cm^{-1} frequency region, markedly different from those of P_{black} and P_{red} and likely due to the presence of chemical bonds involving both P and N. In particular, Product 2 shows two narrow bands at 545 and 725 cm^{-1} and a weaker band centered at 355 cm^{-1} and contained N−H functionalities in the 2850−3500 cm^{-1} frequency range. The presence of both phonon and internal modes suggests Product 2 to be a molecular solid. Finally, Product 1 exhibits a complex and detailed Raman spectrum with narrow bands in the low-frequency region. Neither P−H nor N−H Raman bands were found in Product 1 which could be roughly identified as a covalent solid of P_xN_y composition. Both products 1 and 2 were recovered at ambient conditions.

To improve the assignment of the reaction products, the Raman spectra of Products 1 and 2 were compared with those of several different P_xN_y and $H_xP_yN_z$ systems reported in the literature, like phosphorus nitride imides (general formula HP_xN_y, featuring only P−N and N−H bonds) and phosphorus nitrides (general formula P_xN_y). Figure 7 reports the Raman spectra of the products of P_{red}/NH_3 reaction together with those of partially crystalline P_3N_5 (a mixture of amorphous and α phases of this compound),[55−59] β-HP_4N_7,[60] and three different allotropes of HPN_2: crystalline α-HPN_2,[61] β-HPN_2,[62] and amorphous a-HPN_2.[61] Product 1 shows a low-frequency spectral region closely similar to P_3N_5,[55] consistent with the absence of Raman bands related to P−H and N−H functionalities (see Raman maps, Figures 5 and 6).

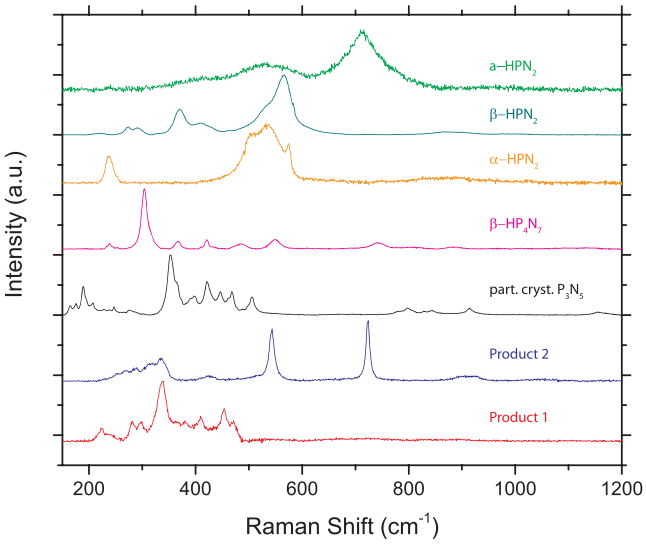

Figure 7. Comparison between the Raman spectra of Product 1 (red trace) and Product 2 (blue trace) with the spectra of several different compounds of general formulas $H_xP_yN_z$ and P_xN_y in the low-frequency region at ambient conditions. The spectra were vertically shifted for the sake of clarity and normalized to their most intense peak.

X-ray Diffraction Results. Due to the structured profiles featuring sharp bands in the low-frequency region, it is reasonable to consider Product 1 and Product 2 as crystalline. Additional information for their identification can be gained by XRD analysis. A synchrotron PXRD mapping was performed on the solid portion of the sample at 0.6 GPa and at ambient conditions. Figure 8 reports a typical diffraction image from the sample and the related integrated pattern acquired at ambient pressure. The two optical images with the superimposed grids graphically summarize the results of the two XRD mappings. The diffraction images consist of spotty patterns, indicating that the recovered solid product was made up of single-crystalline domains of similar dimensions. The integrated peak intensities varied across the sample, likely due to the different orientations of the crystalline domains. The PXRD patterns were acquired at 0.6 GPa and at ambient pressure over a 100 × 80 μm^2 mesh with a spacing of 10 μm, for a total of 80 patterns (20 s each). Only one XRD pattern was found, corresponding to a single phase of a single-crystalline, nonoriented product, with a spatial distribution nicely superimposed with the points where, according to the Raman mapping, mainly product 2 was identified. In the following XRD data analysis, we summed all the 80 diffraction patterns of a mesh at a given pressure to average the different orientations of the crystallites and to attempt to reproduce a powder pattern.

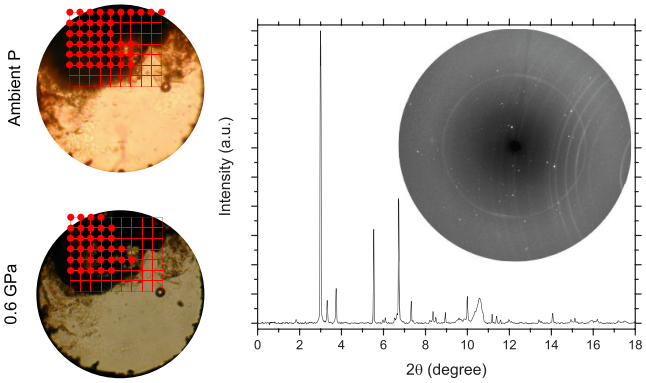

Figure 8. Left: XRD mapping of the solid products obtained after the irradiation of the P_{red}/NH_3 sample at 0.6 GPa (bottom) and recovered after releasing pressure (top). The map consists of an 8 × 10 matrix with 10 μm spatial resolution (red grids). The red solid circles indicate the points on the grid where a diffraction pattern from the sample was detected. Right: a typical XRD pattern of the solid product at ambient pressure acquired in one of the red solid circles and the related diffraction image showing spot reflections instead of diffuse rings (the scattering from the gasket at $2\theta \sim 10.5°$ and secondary scattering from the diffracted beam are also appreciable). The patterns were measured at the ESRF-ID27 High-Pressure dedicated beamline, with X-ray wavelength λ = 0.3738 Å.

Assignment of Product 2 as $P_3N_3(NH_2)_6{\cdot}(NH_3)_{0.5}$. The summed XRD patterns of our product, reported in Figure 9,

https://dx.doi.org/10.1021/acs.jpcc.9b11462
J. Phys. Chem. C XXXX, XXX, XXX−XXX

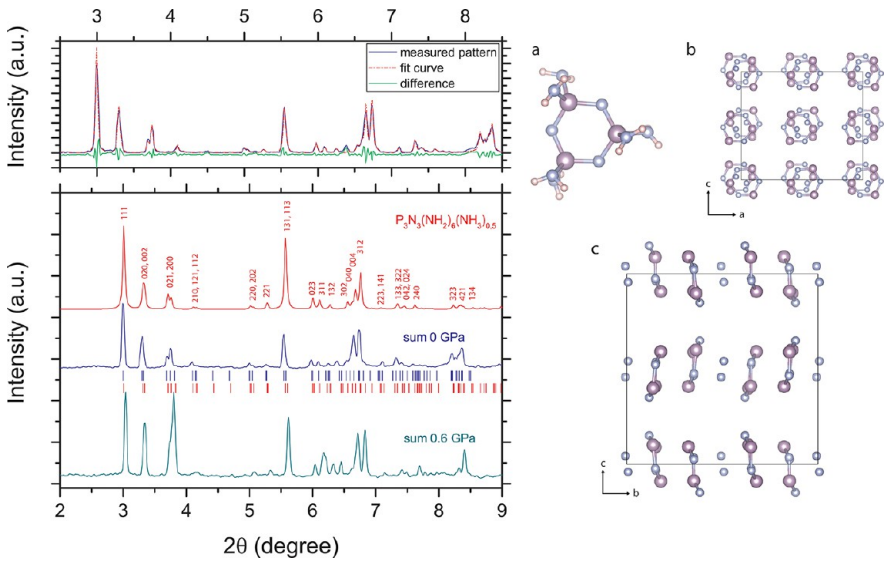

Figure 9. Bottom Left: Comparison among the XRD integrated patterns of the recovered products from the high-pressure photoinduced reactivity of P_{red}/NH_3 at 0.6 GPa (dark cyan trace) and at ambient conditions (blue trace) with the XRD pattern of $P_3N_3(NH_2)_6{\cdot}(NH_3)_{0.5}$ (red trace), generated from the CIF file by Jacobs et al.[63] according to the X-ray wavelength used in our experiment (λ = 0.3738 Å) and normalized to the most intense peak. The CIF file of $P_3N_3(NH_2)_6{\cdot}(NH_3)_{0.5}$ was deposited in 1991 by Jacobs et al.[63] on the Cambridge Crystallographic Data Centre (CCDC), with deposition number 1282091, and the diffraction peaks are indexed according to these structural data. The patterns of the P_{red}/NH_3 product have been obtained by adding the 80 patterns acquired on the grid matrix of Figure 8 for each pressure and then by normalizing them to the most intense peak (excluding the gasket reflection at 10.5 degrees, not shown in this picture). The two series of bars refer to the *hkl* reflections for Product 2 after Pawley fit (blue) and for the $P_3N_3(NH_2)_6{\cdot}(NH_3)_{0.5}$ phase[63](red). Top Left: example of the Pawley fit (red dotted profile) performed on summed XRD patterns from Product 2 at ambient pressure (blue) together with the difference plot (green). Right: (a) the structure of the cyclic unit of $P_3N_3(NH_2)_6$, where pink, violet, and blue spheres, respectively, represent H, P, and N atoms; (b) and (c) two different projections of the crystalline unit cell of the P_3N_3 rings together with the intercalated NH_3 molecules (all the H atoms are omitted for the sake of clarity) along *b* (b) and *a* axes (c). These images were elaborated using the VESTA software,[64] starting from the CIF file provided by Jacobs and coauthors.[63]

present a remarkable similarity to that of hexamminecyclotriphosphazene hemiammonia. This is a crystalline molecular solid of chemical formula $P_3N_3(NH_2)_6{\cdot}(NH_3)_{0.5}$, previously obtained only from white phosphorus in the presence of NH_3 through a disproportion reaction at about 0.5 GPa and temperatures above 523 K, together with PH_3 as a byproduct,[63] according to the following equation:

$$2P_4 + 9.5NH_3 \rightarrow P_3N_3(NH_2)_6{\cdot}(NH_3)_{0.5} + 5PH_3$$

As described by Jacobs and coauthors,[63] each $P_3N_3(NH_2)_6{\cdot}(NH_3)_{0.5}$ unit contains a six-membered ring, a cyclic $P_3N_3(NH_2)_6$ subunit made up of alternating P and N atoms in chain conformation: two $-NH_2$ groups are attached to every P atom in the ring (Figure 9). NH_3 molecules are intercalated between the rings, with these being arranged in pairs held by hydrogen bonds. $P_3N_3(NH_2)_6{\cdot}(NH_3)_{0.5}$ crystallizes in space group *Pbca* (no. 61) with 8 formula units per unit cell and lattice parameters a = 11.395 Å, b = 12.935 Å, and c = 12.834 Å, corresponding to a cell volume of V = 1891.69 Å^3. The sums of the diffraction patterns from Product 2 both at 0.6 GPa and at ambient pressure were analyzed through a Pawley fit with background subtraction using Chebyschev polynomial functions. The results, showing that our experimental diffraction pattern can be indexed by the unit cell of $P_3N_3(NH_2)_6{\cdot}(NH_3)_{0.5}$ as reported by Jacobs,[63] are presented in Figure 9 together with the expected and refined 2θ positions of the *hkl* reflections. Figure 9 reports the results of the fit for the ambient pressure pattern of Product 2 (the results for the 0.6 GPa pattern were totally similar). We observed a very good match of the refined *hkl* reflections of the recovered product at ambient pressure with those of $P_3N_3(NH_2)_6{\cdot}(NH_3)_{0.5}$ obtained by the Jacobs structure in the same pressure conditions. Our refined lattice parameters a = 11.4277(22) Å, b = 12.9977(24) Å, and c = 12.8879(18) Å and the resulting unit cell volume V = 1912.3(5) Å^3 are in good agreement with the literature ones, provided by Jacobs[63] and reported above in the text. In conclusion, considering that the diffraction pattern for the product was found in a good superimposition with the same region where Product 2 was identified by means of Raman spectra, it is reasonable to assign Product 2 as $P_3N_3(NH_2)_6{\cdot}(NH_3)_{0.5}$.

A further confirmation for the assignment of Product 2 comes from the vibrational spectra. Figure 10 reports the FTIR spectra of the products of the P_{red}/NH_3 reaction acquired in this study before and after releasing pressure together with the ambient pressure IR spectrum of $P_3N_3(NH_2)_6{\cdot}(NH_3)_{0.5}$, taken and adapted from the paper of Jacobs et al.,[63] where a complete assignment of the spectrum is reported.

Several absorption bands observed in the reaction product mixture of our experiment showed remarkable agreement with the absorption spectrum of $P_3N_3(NH_2)_6{\cdot}(NH_3)_{0.5}$: in particular, the bands at 930 cm^{-1} and at about 1170 cm^{-1}, related to P−N groups; a peak at 1575 cm^{-1}, assigned to N−H bending modes; and, finally, the weak, large peak at 2600 cm^{-1} and the region of the N−H stretching above 3000 cm^{-1}, that strictly reminded the spectra of P_{red}/NH_3 reaction products. As reported by Allcock,[65] the two bands at about 930 and 1170 cm^{-1} are characteristic of cyclic phosphazenes. Despite the huge debate about the actual presence of formal P═N double bonds in cyclic phosphazenes, which stimulated different

https://dx.doi.org/10.1021/acs.jpcc.9b11462
J. Phys. Chem. C XXXX, XXX, XXX−XXX

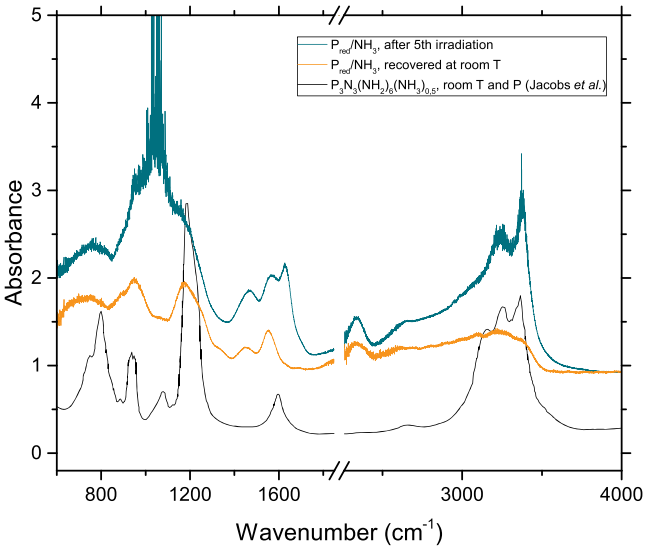

Figure 10. Comparison between the IR absorption spectra of the reaction product of the P_{red}/NH_3 mixture and the IR spectrum of $P_3N_3(NH_2)_6\cdot(NH_3)_{0.5}$.[63] From top to bottom: IR spectrum of the product from P_{red}/NH_3 after the fifth irradiation (cyan trace); IR spectrum of the product from P_{red}/NH_3 recovered at ambient pressure and temperature (orange trace); digitized IR spectrum of $P_3N_3(NH_2)_6\cdot(NH_3)_{0.5}$ in KBr (from ref 63, black trace). The spectra were vertically shifted for the sake of clarity, and therefore their absorbance units have to be intended as relative. The wavenumber axis break excludes the region where the saturating absorption of the diamond anvils occurs.

papers from both the experimental[66,67] and the theoretical point of view[68,69] to opt for different assignments of these vibrational bands, a discussion about the nature of P−N bonds in these compounds lies beyond the purposes of this manuscript: following the textbook by Allcock, the 930 cm^{-1} band can be assigned to symmetric P−N−P stretching modes and while the 1170 cm^{-1} band to antisymmetric stretching modes or the degenerate ring-stretching mode of P−N−P groups.[65] Furthermore, in addition to the bands due to $P_3N_3(NH_2)_6\cdot(NH_3)_{0.5}$, the IR spectrum of our product mixture featured also bands related to P−H functionalities in Product 3 (for example, the weak band at about 2345 cm^{-1}). Indeed our FTIR spectra probed the whole sample area and contained contributions from all the products. It is thus not possible to exclude that some of the same spectral signatures correlated to $P_3N_3(NH_2)_6\cdot(NH_3)_{0.5}$, identified with Product 2, could at the same time contain contributions due to analogous functionalities eventually present also in Product 1, whose actual stoichiometry remains unknown.

In conclusion, as Product 1 is concerned, the presence of only low-frequency bands in its Raman spectrum suggests its assignment to a covalent and nonmolecular extended solid product of general formula (P_xN_y). As Product 2 is concerned, its Raman spectrum, not matching with that of any other known $H_xP_yN_z$ compound, features a very different profile, with low-frequency phonons and distinct high-frequency bands consistent with the internal modes of molecular vibrations, indicating structural differences with respect to Product 1. The XRD patterns of the product mixture that were mainly spatially located in the same region of the sample where the Raman spectra of Product 2 were observed were found to be in fair agreement with the XRD pattern of crystalline $P_3N_3(NH_2)_6\cdot(NH_3)_{0.5}$. This assignment was also supported by the comparison of the FTIR spectrum of the reaction products with that of $P_3N_3(NH_2)_6\cdot(NH_3)_{0.5}$. Unfortunately, no Raman spectrum for $P_3N_3(NH_2)_6\cdot(NH_3)_{0.5}$ has been reported in the literature so far, making a comparison of the Raman profiles not possible at this stage. To the best of our knowledge, the ones reported in this work are the first Raman spectra published in the literature for $P_3N_3(NH_2)_6\cdot(NH_3)_{0.5}$. Further experimental and theoretical efforts should be devoted to better characterize Product 1 (P_xN_y).

■ CONCLUSIONS

A comparison between the high-pressure photoinduced reactivity of amorphous P_{red} and crystalline P_{black} in the presence of NH_3 has been established, with the purpose of correlating the structural and reactive properties of these two allotropes. The products have been characterized by means of FTIR and Raman spectroscopy and synchrotron X-ray diffraction.

A higher reactivity was observed in the case of P_{red} compared to P_{black}, possibly suggesting the persistence of the layered structure and thus opening new routes for the edge functionalization of phosphorene layers before further exfoliation. Like in the case of H_2O[70−72] and EtOH,[73−75] optical pumping of the excited electronic states of NH_3 by two-photon absorption of near-UV light under mild pressure conditions (accessible to the current industrial technology) was able to activate chemical reactivity and to induce the transformation of the starting P_{red}/NH_3 sample into a heterogeneous mixture of products where fluid bubbles and three solids, indicated as Products 1, 2, and 3, have been identified. Micro-Raman spectroscopy revealed that the fluid bubbles mainly contain H_2 and PH_3. Product 3, amorphous and containing P−H functionalities, was found to be unstable if exposed to atmospheric moisture, readily transforming into mainly H_3PO_3. Product 1 and Product 2 are solid materials recoverable at ambient conditions. Product 1 is a novel previously unreported covalent solid material with P_xN_y composition. No further stoichiometric indications could be evinced from our data, and it was not even possible to rule out that Products 1 and 3 could somewhat be intermediate in the synthesis of Product 2. Product 2 contains P−N and N−H bonds and can be identified as $P_3N_3(NH_2)_6\cdot(NH_3)_{0.5}$, a crystalline molecular compound previously obtained only by the disproportion reaction of white phosphorus in the presence of NH_3 at low pressure.[63] To the best of our knowledge, this work represents the first report about the synthesis of such cyclic phosphazenes obtained at room temperature and 0.8 GPa only using UV light as a reaction trigger and starting from elemental red phosphorus and ammonia, according to the following equation:

$$14P_{red} + 19NH_3 \xrightarrow[25°C,0.8\ GPa]{\lambda \simeq 350\ nm} 2P_3N_3(NH_2)_6\cdot(NH_3)_{0.5} + 8PH_3 + H_2$$

The results of this study confirmed the incorporation of the N-bearing fragments originating from the high-pressure photodissociation of NH_3, which acted here as both a reactant and a photoactivator.[29]

Moreover, the conversion of P_{red} into $P_3N_3(NH_2)_6\cdot(NH_3)_{0.5}$, H_2 and PH_3 in the total absence of solvents, catalysts, and radical initiators under mild pressure conditions accessible to

https://dx.doi.org/10.1021/acs.jpcc.9b11462
J. Phys. Chem. C XXXX, XXX, XXX−XXX

current industrial techniques could represent an appealing chemical process potentially combining the synthesis of cyclophosphazenes, which have a large variety of possible applications as cores for polymers or dendrimers or also as starting substrates for supramolecular chemistry and nanostructured materials, with the synthesis of H_2, molecular hydrogen being one of most interesting and promising energy vectors.

■ AUTHOR INFORMATION

Corresponding Author

Demetrio Scelta − *LENS, European Laboratory for Non-linear Spectroscopy, Sesto Fiorentino, Italy, and Institute of Chemistry of OrganoMetallic Compounds, National Research Council of Italy, Sesto Fiorentino, Italy;* orcid.org/0000-0002-4856-0125; Email: scelta@lens.unifi.it

Other Authors

Adhara Baldassarre − *LENS, European Laboratory for Non-linear Spectroscopy, Sesto Fiorentino, Italy, and Università Degli Studi di Firenze, Sesto Fiorentino, Italy*

Manuel Serrano-Ruiz − *Institute of Chemistry of OrganoMetallic Compounds, National Research Council of Italy, Sesto Fiorentino, Italy*

Alexey Marchuk − *Ludwig-Maximilians-Universität München, München, Germany*

Sebastian Vogel − *Ludwig-Maximilians-Universität München, München, Germany*

Wolfgang Schnick − *Ludwig-Maximilians-Universität München, München, Germany;* orcid.org/0000-0003-4571-8035

Maurizio Peruzzini − *Institute of Chemistry of OrganoMetallic Compounds, National Research Council of Italy, Sesto Fiorentino, Italy*

Roberto Bini − *LENS, European Laboratory for Non-linear Spectroscopy, Sesto Fiorentino, Italy, Institute of Chemistry of OrganoMetallic Compounds, National Research Council of Italy, Sesto Fiorentino, Italy, and Università Degli Studi di Firenze, Sesto Fiorentino, Italy;* orcid.org/0000-0002-6746-696X

Matteo Ceppatelli − *LENS, European Laboratory for Non-linear Spectroscopy, Sesto Fiorentino, Italy, and Institute of Chemistry of OrganoMetallic Compounds, National Research Council of Italy, Sesto Fiorentino, Italy;* orcid.org/0000-0002-0688-5167

Complete contact information is available at: https://pubs.acs.org/10.1021/acs.jpcc.9b11462

Notes

The authors declare no competing financial interest.

■ ACKNOWLEDGMENTS

The authors thank the EC through the European Research Council (ERC) for funding the project PHOSFUN "Phosphorene functionalization: a new platform for advanced multifunctional materials" (Grant Agreement No. 670173) through an ERC Advanced Grant. This study was supported also by the Deep Carbon Observatory (DCO) initiative under the project Physics and Chemistry of Carbon at Extreme Conditions, by the Italian Ministero dell'Istruzione, Università e della Ricerca (MIUR) and by Fondazione Cassa di Risparmio di Firenze under the project HP-PHOTOCHEM. The authors acknowledge the European Synchrotron Radiation Facility for provision of synchrotron radiation facilities and are grateful to Dr. Andrew B. Cairns for assistance in using beamline ID27.

■ REFERENCES

(1) Corbridge, D. E. G. *Phosphorus Chemistry, Biochemistry and Technology*, 6th ed.; 2013.

(2) Böcker, S.; Häser, M. Covalent Structures of Phosphorus: A Comprehensive Theoretical Study. *Z. Anorg. Allg. Chem.* **1995**, *621*, 258−286.

(3) Green, J. A Review of Phosphorus-Containing Flame Retardants. *J. Fire Sci.* **1992**, *10*, 470−487.

(4) Zaug, J. M.; Soper, A. K.; Clark, S. M. Pressure-dependent structures of amorphous red phosphorus and the origin of the first sharp diffraction peaks. *Nat. Mater.* **2008**, *7*, 890−899.

(5) Rissi, E. N.; Soignard, E.; McKiernan, K. A.; Benmore, C. J.; Yarger, J. L. Pressure-induced crystallization of amorphous red phosphorus. *Solid State Commun.* **2012**, *152*, 390−394.

(6) Long, L. J.; Guarise, G. B.; Marani, A. Phase transitions of phosphorus at high pressure. *Corsi. Semin. Chim.* **1967**, *5*, 97−104.

(7) Endo, S.; Akahama, Y.; Terada, S.; Narita, S. Growth of Large Single Crystals of Black Phosphorus under High Pressure. *Jpn. J. Appl. Phys.* **1982**, *21*, L482−L484.

(8) Clark, S. M.; Zaug, J. M. Compressibility of cubic white, orthorhombic black, rhombohedral black, and simple cubic black phosphorus. *Phys. Rev. B: Condens. Matter Mater. Phys.* **2010**, *82*, 134111.

(9) Kikegawa, T.; Iwasaki, H.; Fujimura, T.; Endo, S.; Akahama, Y.; Akai, T.; Shimomura, O.; Yagi, T.; Akimoto, S.; Shirotani, I. Synchrotron-radiation study of phase transitions in phosphorus at high pressures and temperatures. *J. Appl. Crystallogr.* **1987**, *20*, 406−410.

(10) Cartz, L.; Srinivasa, S. R.; Riedner, R. J.; Jorgensen, J. D.; Worlton, T. G. Effect of pressure on bonding in black phosphorus. *J. Chem. Phys.* **1979**, *71*, 1718−1721.

(11) Ahuja, R. Calculated high pressure crystal structure transformations for phosphorus. *Phys. Status Solidi B* **2003**, *235*, 282−287.

(12) Bridgman, P. W. Two new modifications of Phosphorus. *J. Am. Chem. Soc.* **1914**, *36*, 1344−1363.

(13) Scelta, D.; Baldassarre, A.; Serrano-Ruiz, M.; Dziubek, K.; Cairns, A. B.; Peruzzini, M.; Bini, R.; Ceppatelli, M. Interlayer Bond Formation in Black Phosphorus at High Pressure. *Angew. Chem., Int. Ed.* **2017**, *56*, 14135−14140.

(14) Peruzzini, M.; Bini, R.; Bolognesi, M.; Caporali, M.; Ceppatelli, M.; Cicogna, F.; Coiai, S.; Heun, S.; Ienco, A.; Benito, I. I.; et al. A Perspective on Recent Advances in Phosphorene Functionalization and Its Applications in Devices. *Eur. J. Inorg. Chem.* **2019**, *2019*, 1476−1494.

(15) Brown, A.; Rundqvist, S. Refinement of the crystal structure of black phosphorus. *Acta Crystallogr.* **1965**, *19*, 684−685.

(16) Chang, K. J.; Cohen, M. L. Structural stability of phases of black phosphorus. *Phys. Rev. B: Condens. Matter Mater. Phys.* **1986**, *33*, 6177−6186.

(17) Scelta, D.; Baldassarre, A.; Serrano-Ruiz, M.; Dziubek, K.; Cairns, A. B.; Peruzzini, M.; Bini, R.; Ceppatelli, M. The p-sc structure in phosphorus: bringing order to the high pressure phases of group 15 elements. *Chem. Commun.* **2018**, *54*, 10554−10557.

(18) Akahama, Y.; Kobayashi, M.; Kawamura, H. Simple-cubic-simple-hexagonal transition in phosphorus under pressure. *Phys. Rev. B: Condens. Matter Mater. Phys.* **1999**, *59*, 8520−8525.

(19) Ceppatelli, M.; Bini, R.; Caporali, M.; Peruzzini, M. High-Pressure Chemistry of Red Phosphorus and Water under Near-UV Irradiation. *Angew. Chem., Int. Ed.* **2013**, *52*, 2313−2317.

(20) Ceppatelli, M.; Fanetti, S.; Bini, R. Photoinduced Reactivity of Red Phosphorus and Ethanol at High Pressure. *J. Phys. Chem. C* **2013**, *117*, 13129−13135.

(21) Ninet, S.; Datchi, F. High pressure-high temperature phase diagram of ammonia. *J. Chem. Phys.* **2008**, *128*, 154508.

(22) Loveday, J. S.; Nelmes, R. J.; Marshall, W. G.; Besson, J. M.; Klotz, S.; Hamel, G. Structure of Deuterated Ammonia IV. *Phys. Rev. Lett.* **1996**, *76*, 74−77.

(23) Bach, A.; Hutchison, J. M.; Holiday, R. J.; Crim, F. F. Vibrational spectroscopy and photodissociation of jet-cooled ammonia. *J. Chem. Phys.* **2002**, *116*, 4955−4961.

(24) Lai, W.; Lin, S. Y.; Xie, D.; Guo, H. Full-dimensional quantum dynamics of $\tilde{A}$-state photodissociation of ammonia: absorption spectra. *J. Chem. Phys.* **2008**, *129*, 154311.

(25) Mordaunt, D. H.; Ashfold, M. N. R.; Dixon, R. N. Photodissociation dynamics of $\tilde{A}$ state ammonia molecules. I. State dependent μ-ν correlations in the $NH_2(ND_2)$ products. *J. Chem. Phys.* **1996**, *104*, 6460−6471.

(26) Vaida, V.; McCarthy, M. I.; Engelking, P. C.; Rosmus, P.; Werner, H.; Botschwina, P. The ultraviolet absorption spectrum of the $\tilde{A}^1A'_2 \leftarrow \tilde{X}^1A_1$ transition of jet-cooled ammonia. *J. Chem. Phys.* **1987**, *86*, 6669−6676.

(27) Chou, S.-L.; Lo, J.-I.; Peng, Y.-C.; Lu, H.-C.; Cheng, B.-M. Electronic and Vibrational Absorption Spectra of NH_2 in Solid Ne. *ACS Omega* **2019**, *4*, 2268−2274.

(28) Ceppatelli, M.; Scelta, D.; Tuci, G.; Giambastiani, G.; Hanfland, M.; Bini, R. Lattice expansion of graphite oxide by pressure induced insertion of liquid ammonia. *Carbon* **2015**, *93*, 484−491.

(29) Ceppatelli, M.; Scelta, D.; Tuci, G.; Giambastiani, G.; Hanfland, M.; Bini, R. High-Pressure Chemistry of Graphene Oxide in the Presence of Ar, N_2, and NH_3. *J. Phys. Chem. C* **2016**, *120*, 5174−5187.

(30) Drozdov, A. P.; Eremets, M. I.; Troyan, I. A.; Ksenofontov, V.; Shylin, S. I. Conventional superconductivity at 203 K at high pressures in the sulfur hydride system. *Nature* **2015**, *525*, 73−76.

(31) Drozdov, A. P.; Kong, P. P.; Minkov, V. S.; Besedin, S. P.; Kuzovnikov, M. A.; Mozaffari, S.; Balicas, L.; Balakirev, F. F.; Graf, D. E.; Prakapenka, V. B.; et al. Superconductivity at 250 K in lanthanum hydride under high pressures. *Nature* **2019**, *569*, 528−531.

(32) Shao, Z.; Duan, D.; Ma, Y.; Yu, H.; Song, H.; Xie, H.; Li, D.; Tian, F.; Liu, B.; Cui, T. Ternary superconducting cophosphorus hydrides stabilized via lithium. *Npj Comput. Mater.* **2019**, *5*, 104.

(33) Sun, Y.; Lv, J.; Xie, Y.; Liu, H.; Ma, Y. Route to a Superconducting Phase above Room Temperature in Electron-Doped Hydride Compounds under High Pressure. *Phys. Rev. Lett.* **2019**, *123*, 097001.

(34) Davids, M. W.; Lototskyy, M.; Malinowski, M.; van Schalkwyk, D.; Parsons, A.; Pasupathi, S.; Swanepoel, D.; van Niekerk, T. Metal hydride hydrogen storage tank for light fuel cell vehicle. *Int. J. Hydrogen Energy* **2019**, *44*, 29263−29272.

(35) Scelta, D.; Ceppatelli, M.; Ballerini, R.; Hajeb, A.; Peruzzini, M.; Bini, R. Spray-loading: A cryogenic deposition method for diamond anvil cell. *Rev. Sci. Instrum.* **2018**, *89*, 053903.

(36) Mao, H. K.; Bell, P. M.; Shaner, J. W.; Steinberg, D. J. Specific volume measurements of Cu, Mo, Pd, and Ag and calibration of the ruby R1 fluorescence pressure gauge from 0.06 to 1 Mbar. *J. Appl. Phys.* **1978**, *49*, 3276−3283.

(37) Syassen, K. Ruby under pressure. *High Pressure Res.* **2008**, *28*, 75−126.

(38) Ceppatelli, M.; Gorelli, F. A.; Haines, J.; Santoro, M.; Bini, R. Probing high-pressure reactions in heterogeneous materials by Raman spectroscopy. *Z. Kristallogr. - Cryst. Mater.* **2014**, *229*, 83−91.

(39) Wojdyr, M. *Fityk*: a general-purpose peak fitting program. *J. Appl. Crystallogr.* **2010**, *43*, 1126−1128.

(40) Bini, R.; Ballerini, R.; Pratesi, G.; Jodl, H. J. Experimental setup for Fourier transform infrared spectroscopy studies in condensed matter at high pressure and low temperatures. *Rev. Sci. Instrum.* **1997**, *68*, 3154−3160.

(41) Mezouar, M.; Crichton, W. A.; Bauchau, S.; Thurel, F.; Witsch, H.; Torrecillas, F.; Blattmann, G.; Marion, P.; Dabin, Y.; Chavanne, J.; et al. Development of a new state-of-the-art beamline optimized for monochromatic single-crystal and powder X-ray diffraction under extreme conditions at the ESRF. *J. Synchrotron Radiat.* **2005**, *12*, 659−664.

(42) Prescher, C.; Prakapenka, V. B. DIOPTAS: a program for reduction of two-dimensional X-ray diffraction data and data exploration. *High Pressure Res.* **2015**, *35*, 223−230.

(43) Toby, B. H.; Von Dreele, R. B. *GSAS-II*: the genesis of a modern open-source all purpose crystallography software package. *J. Appl. Crystallogr.* **2013**, *46*, 544−549.

(44) Gardiner, D. J.; Hester, R. E.; Grossman, W. E. L. Ammonia in the liquid state and in solution: A Raman study. *J. Raman Spectrosc.* **1973**, *1*, 87−95.

(45) Bromberg, A.; Kimel, S.; Ron, A. Infrared spectrum of liquid and crystalline ammonia. *Chem. Phys. Lett.* **1977**, *46*, 262−266.

(46) Holt, J. S.; Sadoskas, D.; Pursell, C. J. Infrared spectroscopy of the solid phases of ammonia. *J. Chem. Phys.* **2004**, *120*, 7153−7157.

(47) Sakashita, M.; Yamawaki, H.; Fujihisa, H.; Aoki, K. Phase Study of NH_3 to 100 GPa by Infrared Absorption. *Koatsuryoku no Kagaku to Gijutsu* **1998**, *7*, 796−798.

(48) Akahama, Y.; Kobayashi, M.; Kawamura, H. Raman study of black phosphorus up to 13 GPa. *Solid State Commun.* **1997**, *104*, 311−315.

(49) Lin-Vien, D.; Colthup, N. B.; Fateley, W. G.; Grasselli, J. G. *The Handbook of Infrared and Raman Characteristic Frequencies of Organic Molecules*; Academic Press, 1991.

(50) Subramaniyam, C. M.; Tai, Z.; Mahmood, N.; Zhang, D.; Liu, H. K.; Goodenough, J. B.; Dou, S. X. Unlocking the potential of amorphous red phosphorus films as a long-term stable negative electrode for lithium batteries. *J. Mater. Chem. A* **2017**, *5*, 1925−1929.

(51) Luo, Z.-Z.; Zhang, Y.; Zhang, C.; Tan, H. T.; Li, Z.; Abutaha, A.; Wu, X.-L.; Xiong, Q.; Khor, K. A.; Hippalgaonkar, K.; et al. Multifunctional 0D-2D Ni_2P Nanocrystals-Black Phosphorus Heterostructure. *Adv. Energy Mater.* **2017**, *7*, 1601285.

(52) Ribeiro, H. B.; Pimenta, M. A.; de Matos, C. J. Raman spectroscopy in black phosphorus. *J. Raman Spectrosc.* **2018**, *49*, 76−90.

(53) Bafile, U.; Ulivi, L.; Zoppi, M.; Barocchi, F. Depolarized-light-scattering spectrum of normal gaseous hydrogen at low density and a temperature of 297 K. *Phys. Rev. A: At., Mol., Opt. Phys.* **1988**, *37*, 4133−4144.

(54) Ulivi, L.; Zoppi, M.; Gioè, L.; Pratesi, G. Molecular hydrogen internuclear distance in high-pressure fluid and solid phases at room temperature. *Phys. Rev. B: Condens. Matter Mater. Phys.* **1998**, *58*, 2383−2386.

(55) Vepřek, S.; Iqbal, Z.; Brunner, J.; Schärli, M. Preparation and properties of amorphous phosphorus nitride prepared in a low-pressure plasma. *Philos. Mag. B* **1981**, *43*, 527−547.

(56) Schnick, W.; Lücke, J.; Krumeich, F. Phosphorus Nitride P_3N_5: Synthesis, Spectroscopic, and Electron Microscopic Investigations. *Chem. Mater.* **1996**, *8*, 281−286.

(57) Landskron, K.; Huppertz, H.; Senker, J.; Schnick, W. High-Pressure Synthesis of γ-P_3N_5 at 11 GPa and 1500°C in a Multianvil Assembly: a Binary Phosphorus(V) Nitride with a Three-Dimensional Network Structure from PN_4 Tetrahedra and Tetragonal PN_5 Pyramids. *Angew. Chem., Int. Ed.* **2001**, *40*, 2643−2645.

(58) Landskron, K.; Huppertz, H.; Senker, J.; Schnick, W. Multianvil-Synthese, Pulver-Röntgenstrukturanalyse, ^{31}P-MAS-NMR- und FTIR-Spektroskopie sowie Materialeigenschaften von γ-P_3N_5, einer Hochdruckphase von binärem Phosphor(V)-nitrid mit verzerrt quadratischen PN_5-Pyramiden und PN_4-Tetraedern. *Z. Anorg. Allg. Chem.* **2002**, *628*, 1465−1471.

(59) Horstmann, S.; Irran, E.; Schnick, W. Synthesis and Crystal Structure of Phosphorus(V) Nitride α-P_3N_5. *Angew. Chem., Int. Ed. Engl.* **1997**, *36*, 1873−1875.

https://dx.doi.org/10.1021/acs.jpcc.9b11462
J. Phys. Chem. C XXXX, XXX, XXX−XXX

(60) Baumann, D.; Schnick, W. High-Pressure Polymorph of Phosphorus Nitride Imide HP_4N_7 Representing a New Framework Topology. *Inorg. Chem.* **2014**, *53*, 7977−7982.
(61) Schnick, W.; Lücke, J.; Darstellung, K. ristallstruktur und IR-spektroskopische Untersuchung von Phosphor(V)-nitrid-imid, HPN_2. *Z. Anorg. Allg. Chem.* **1992**, *610*, 121−126.
(62) Marchuk, A.; Pucher, F. J.; Karau, F. W.; Schnick, W. A High-Pressure Polymorph of Phosphorus Nitride Imide. *Angew. Chem., Int. Ed.* **2014**, *53*, 2469−2472.
(63) Jacobs, H.; Krichgässner, R. Hexamincyclotriphosphazenhe-miammoniakat, $P_3N_3(NH_2)_6 \cdot 0{,}5\ NH_3$, ein Produkt der Hochdruck-ammonolyse von weißem Phosphor. *Z. Anorg. Allg. Chem.* **1990**, *581*, 125−134.
(64) Momma, K.; Izumi, F. *VESTA3* for three-dimensional visualization of crystal, volumetric and morphology data. *J. Appl. Crystallogr.* **2011**, *44*, 1272−1276.
(65) Allcock, H. R. *Phosphorus-nitrogen Compounds- Cyclic, Linear, and High Polymeric Systems*, 1st ed.; Academic Press, 1972.
(66) Allen, F. H.; Kennard, O.; Watson, D. G.; Brammer, L.; Orpen, A. G.; Taylor, R. Tables of bond lengths determined by X-ray and neutron diffraction. Part 1. *J. Chem. Soc., Perkin Trans. 2* **1987**, *2*, S1−S19.
(67) Bolboaca, M.; Stey, T.; Murso, A.; Stalke, D.; Kiefer, W. P-N Bond Length Alterations Monitored by Infrared Absorption and Fourier Transform Raman Spectroscopy in Combination with Density Functional Theory Calculations. *Appl. Spectrosc.* **2003**, *57*, 970−976.
(68) Luaña, V.; Pendás, A. M.; Costales, A.; Carriedo, G. A.; García-Alonso, F. J. Topological Analysis of Chemical Bonding in Cyclophosphazenes. *J. Phys. Chem. A* **2001**, *105*, 5280−5291.
(69) Jancik, V.; Cortés-Guzmán, F.; Herbst-Irmer, R.; Matínez-Otero, D. Is Hexachloro-cyclo-triphosphazene Aromatic? Evidence from Experimental Charge Density Analysis. *Chem. - Eur. J.* **2017**, *23*, 6964−6968.
(70) Ceppatelli, M.; Bini, R.; Schettino, V. High-pressure photo-dissociation of water as a tool for hydrogen synthesis and fundamental chemistry. *Proc. Natl. Acad. Sci. U. S. A.* **2009**, *106*, 11454−11459.
(71) Ceppatelli, M.; Bini, R.; Schettino, V. High-Pressure Reactivity of Model Hydrocarbons Driven by Near-UV Photodissociation of Water. *J. Phys. Chem. B* **2009**, *113*, 14640−14647.
(72) Ceppatelli, M.; Bini, R.; Schettino, V. High-pressure reactivity of clathrate hydrates by two-photon dissociation of water. *Phys. Chem. Chem. Phys.* **2011**, *13*, 1264−1275.
(73) Ceppatelli, M.; Fanetti, S.; Citroni, M.; Bini, R. Photoinduced Reactivity of Liquid Ethanol at High Pressure. *J. Phys. Chem. B* **2010**, *114*, 15437−15444.
(74) Fanetti, S.; Ceppatelli, M.; Citroni, M.; Bini, R. Changing the Dissociative Character of the Lowest Excited State of Ethanol by Pressure. *J. Phys. Chem. B* **2011**, *115*, 15236−15240.
(75) Fanetti, S.; Ceppatelli, M.; Citroni, M.; Bini, R. High-Pressure Photoinduced Reactivity of CH_3OH and CD_3OH. *J. Phys. Chem. C* **2012**, *116*, 2108−2115.

https://dx.doi.org/10.1021/acs.jpcc.9b11462
J. Phys. Chem. C XXXX, XXX, XXX−XXX